SSRG International Journal of Civil Engineering
ISSN: 2348-8352/ https://doi.org/10.14445/23488352/IJCE-V12I2P106

Volume 12 Issue 2, 51-70, Febuary 2025
© 2025 Seventh Sense Research Group®

Original Article

Assessment of Variability in Glacier and Snow Melt Runoff for Alaknanda River Basin Using Spatially Distributed Snow and Glacier Melt Runoff Model (SDSGRM)

R. Murtem[1], N. Shiu[2], A. Bhadra[3], A. Bandyopadhyay[4]

[1,2,3,4]*Department of Agricultural Engineering NERIST, Arunachal Pradesh, India.*

[1]*Corresponding Author : rimummurtem1@gmail.com*

Received: 08 December 2024 Revised: 09 January 2025 Accepted: 10 February 2025 Published: 27 February 2025

Abstract *- Evaluating snowmelt, glacier melt, and rainfall-induced runoff is required to understand hydrological dynamics in glaciated basins. However, challenges arise due to their remote nature and scarce data availability. The Spatially Distributed Snow and Glacier Melt Runoff Model (SDSGRM) was applied in the Alaknanda River Basin to estimate streamflow, incorporating daily variables such as temperature, precipitation, snow cover, and wind speed. Model calibration (2006-2010) and validation (2012-2014) utilized multiple melt depth estimation techniques. During calibration, Modelling Efficiency (ME) values ranged between 0.51 and 0.77, with R^2 surpassing 0.6, while the Coefficient of Residual Mass (CRM) varied from -0.01 to 0.2. Validation exhibited comparable results, with ME and R^2 remaining above 0.5 and 0.6, respectively, and CRM fluctuating between -0.08 and 0.18. The energy balance method generally outperformed the others. Average runoff contributions were 93.19% from Rainfall Water Yield (RWY), 6.58% from Snow Water Yield (SWY), and 0.17% from Glacier Water Yield (GWY). Given its acceptable performance, SDSGRM proves to be an effective tool for analyzing the runoff contributions in glaciated, data-scarce basins and assessing climate change's influence.*

Keywords *- SDSGRM, Rainfall, Snowmelt, Glacier-melt, Runoff.*

1. Introduction

A significant portion of the South Asian population depends on runoff from the Himalayan River basin, a primary freshwater source. The Himalayas hold approximately 33,200 sq. km of snow and ice, with glacier systems situated at elevations ranging from 4,300 to 5,800 m.a.s.l [1]. These glaciers function as natural reservoirs, releasing meltwater into major river systems, particularly during dry seasons [2]. The hydrology in high-terrain environments is largely governed by the cryosphere, where snow and ice temporarily retain water before gradually releasing it as meltwater [3]. However, this delicate balance faces increasing threats due to global warming, which is predicted to alter runoff patterns, shift precipitation distribution, and intensify extreme hydrological events [4-6]. Despite the importance of water resources derived from snow and ice, maintaining hydrological stability and accurately quantifying their contributions to streamflow remains challenging. This difficulty is particularly evident in ungauged basins, where limited observational data, often due to remoteness and difficult terrain, hinders direct measurements [7]. Traditional hydrological models often struggle to represent the complex interactions between precipitation, snowmelt, and glacier melt, leading to uncertainties in streamflow predictions [8]. Furthermore, past research has primarily examined snowmelt and glacier melt separately instead of integrating their combined influence on river runoff [9, 10]. The lack of a comprehensive modelling framework hampers accurate predictions of efficient future water resource management and utilization strategies to address water availability challenges to counter-measure climate change. [11].

Advancements in geospatial technology have opened new possibilities for addressing knowledge gaps in snowmelt runoff modelling. With enhanced access to high-resolution satellite data and reanalysis datasets, hydrological models can now be refined to simulate runoff patterns more accurately, even in areas with scarce data [12, 13]. Several models have been designed to estimate runoff driven by snowmelt, each with strengths and limitations.

The degree day-based model, the Snowmelt Runoff Model (SRM), is structured to estimate snowmelt contribution to streamflow in high-altitude river basins [14]. The challenges of modelling snowmelt in the Himalayas face challenges due to the significant variability in snow

This is an open access article under the CC BY-NC-ND license (http://creativecommons.org/licenses/by-nc-nd/4.0/)

parameters [15]. HBV, SRM, and WinSRM are some of the widely applied runoff-simulating models [16]. While these models have demonstrated effectiveness in runoff simulation, they provide limited insights into the specific snow characteristics influencing the snowmelt process. The Spatially Distributed Snowmelt Runoff Model (SDSRM) is a hydrological model driven by temperature and has been effectively utilized in the western and eastern Himalayas to analyze variations in snow parameters and simulate spatially distributed snowmelt runoff from spatially variable DDF. The Spatially Distributed Snowmelt and Glacier Melt Runoff Model (SDSGRM) is a recent advancement on SDSRM designed to address the challenges in ungauged and semi-gauged catchments. SDSGRM integrates additional parameters, including radiation-based components and energy balance methods, to refine snowmelt depth estimations. Unlike traditional temperature index models, SDSGRM provides multiple techniques, such as a temperature-based index method, radiation-temperature index technique, advection-driven index approach, and an enhanced energy balance approach. Additionally, a specialized glacier module is designed to simulate glacier melt runoff. This module also generates daily glacier area data, improving assessments of glacier melt contributions to streamflow. Alaknanda River Basin is heavily influenced by snow and glacier melt. Meltwater from these sources accounts for approximately 20 to 30 % of the basin's total annual flow [17]. Long-term hydrological studies indicate that between 1994 and 2020, glacier shrinkage in the Upper Alaknanda Basin has significantly impacted the contributions from meltwater, raising concerns about future water availability [18]. This research aims to provide a detailed evaluation of both seasonal and long-term variability in runoff contributions in the Alaknanda Basin. Acceleration in climate change is impacting glacier retreat and altering precipitation patterns. This research offers insights for future water resource management, disaster preparedness, and climate adaptation in high-altitude river basins.

2. Data and Methodology

2.1. Alaknanda River Basin

The Alaknanda River drains into Ganga, originating in Uttarakhand, where the Bhagirathi, Kharak, and Satopanth glaciers merge. The Alaknanda River Basin spans roughly 4,500 sq.km. The geographical extent of the basin is from 79°45' to 80°00' E longitude and 30°30' to 31°10' N latitude, and an elevation range between 1,365 and 7,811 m.a.s.l. The Indian summer monsoon significantly influences the Alaknanda basin, bringing an average annual rainfall of approximately 1,185 mm between June and September. During winter, the region experiences substantial snowfall. The study area comprises high mountain ranges in the northwest and northeast, which remain snow-covered and glaciers for most of the year. The perennial flow of tributaries in the basin is primarily sustained by seasonal rainfall, snowmelt, and glacier melt. Figure 1 illustrates the study area.

2.2. Data Acquisition

2.2.1. Satellite Data

Snow cover and albedo data were obtained from the Terra Snow Cover Daily L3 Global 500m Grid, created and distributed by the National Snow and Ice Data Center (NSIDC) through NASA's Distributed Active Archive Center (DAAC) (https://search.earthdata.nasa.gov/search). Surface albedo (MCD43A3) data for each basin were retrieved from the Application for Extracting and Exploring Analysis Ready Samples (AppEEARS), also distributed by DAAC and managed by the Land Processes Distributed Active Archive Center (LPDAAC) (https://appeears.earthdatacloud.nasa.gov/). Additionally, a 30-meter resolution Digital Elevation Model (DEM) from the Advanced Spaceborne Thermal Emission and Reflection Radiometer (ASTER) was acquired from NASA.

2.2.2. Reanalysis Data

ERA5 single-level datasets were utilized to obtain data on total precipitation, maximum and minimum temperatures measured at two meters, wind v- and u-components, dew point temperature measured at ten meters, snow layer temperature, and skin temperature. ERA5 pressure-level datasets provided maximum and minimum relative humidity, whereas sunshine duration data came from ERA-Interim (https://cds.climate.copernicus.eu).

2.3. Data Pre-Processing and Synthesis of Snow and Glacier Parameters Using SDSGRM

Acquired satellite data were initially projected onto the UTM 44N zone, trimmed to the research region, and converted into ASCII format. Reanalysis data were downloaded in NetCDF format using QGIS 3.10.1 and transformed into GeoTIFF files. The GeoTIFF files were then resampled and reprojected to match MODIS resolution, ensuring alignment within the same UTM 44N zone. Pixel values within the study area were extracted using the 'extract by mask' tool and converted into ASCII format for input into SDSGRM. A flowchart illustrating the data preprocessing steps is presented in Figure 2. The preprocessed data were then combined to synthesize snow and glacier parameters using SDSGRM. A simplified flowchart of SDSGRM is shown in Figure 3.

2.4. SDSGRM Validation and Calibration

The snow year concept was implemented to capture hydrological conditions across multiple years, ensuring that snow precipitation stored within the snowpack was accounted for until its eventual melt in spring or summer rather than being immediately factored into streamflow. The SDSGRM was calibrated using data from 2006 to 2010 and validated against observed records spanning 2012 to 2014. The model's effectiveness was assessed through statistical indicators, including the Coefficient of Determination (R^2), Mean Error (ME), Standard Error of Estimate (SEE), and Coefficient of Residual Mass (CRM).

Calibration was conducted using four melt depth index methods, selected based on regional data availability, computational feasibility, and dominant melt-driving influences. These methods included the temperature-based index method, the radiation-temperature index technique, the advection-driven index approach, and an enhanced energy balance approach, as outlined in Tables 2, 3, 4, and 5.

2.4.1. Temperature Index Method

The critical temperature was set at 1.2°C to define the threshold for snowmelt initiation. The storage coefficient was calibrated at 0.04, representing the snowpack's capacity to retain water before contributing to runoff. Runoff coefficients were adjusted for rain (0.5), snowmelt (0.75), and glacier melt (0.009-0.01) to capture variations in water input. Ice melt parameters included an ice temperature melt factor (2.0) and an ice radiation melt factor (0.025). Sublimation factors were set at 0.5 (June 21) and 0.4 (December 21) to account for seasonal atmospheric moisture loss. The meltwater refreezing ratio (0.55) and basal coefficient (0.0015) were adjusted.

2.4.2. Radiation-Temperature Index Method

This method incorporated temperature and solar radiation to enhance snowmelt simulations. The critical temperature remained at 1.2°C, with a storage coefficient 0.04. The model accounted for radiation influences through a transmittance value of 0.099 and a sky-view fraction of 0.172 to refine solar energy distribution. Runoff coefficients were optimized for rain (0.5-0.55), snowmelt (0.65-0.8), and glacier melt (0.009-0.01). Ice melt calibration included an ice temperature melt factor (2.0) and an ice radiation melt factor (0.025). Sublimation factors were set at 0.5 (June 21) and 0.4–0.5 (December 21), while the meltwater refreezing ratio (0.95–0.98) and basal coefficient (0.0015) were optimized for hydrological accuracy.

2.4.3. Advection-Driven Index Method

This approach accounted for additional heat transfer mechanisms influencing snowmelt. The critical temperature (1.2°C) and storage coefficient (0.04) remained unchanged. Runoff coefficients were adjusted for rain (0.5), snowmelt (0.75), and glacier melt (0.01-0.02). The thermal quality of snow (0.95) was incorporated to refine melt rate estimations. Ice melt parameters included an ice temperature melt factor (2.0) and an ice radiation melt factor (0.025). Sublimation factors were set at 0.5 (June 21) and 0.4 (December 21), while the meltwater refreezing ratio (0.95-0.96) and basal coefficient (0.0015) were calibrated for improved accuracy.

2.*4.4. Energy Balance Method*

This method integrates multiple energy fluxes that affect snow and glacier melt. The critical temperature (1.2°C) and storage coefficient (0.04) were retained. Radiative inputs were incorporated using transmittance (0.099) and a sky-view fraction (0.172). Runoff coefficients were assigned for rain (0.5), snowmelt (0.75), and glacier melt (0.006-0.01). Ice melt was parameterized with an ice temperature melt factor (2.0) and an ice radiation melt factor (0.025). Sublimation effects were accounted for using sublimation factors of 0.5 (June 21) and 0.4 (December 21), while the meltwater refreezing ratio (0.92-0.95) and basal coefficient (0.0015) were adjusted for precise runoff estimation.

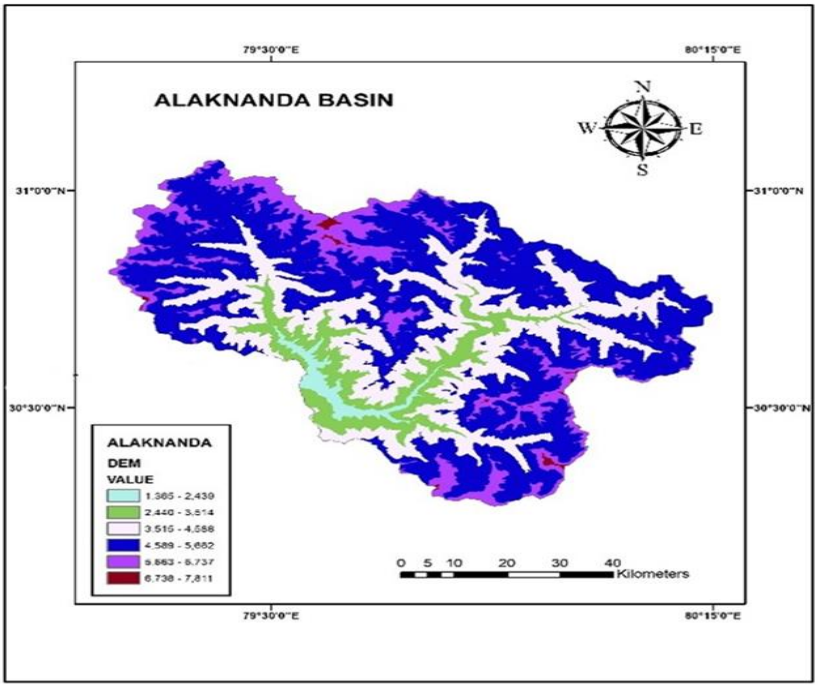

Fig. 1 DEM of Alaknanda river basin

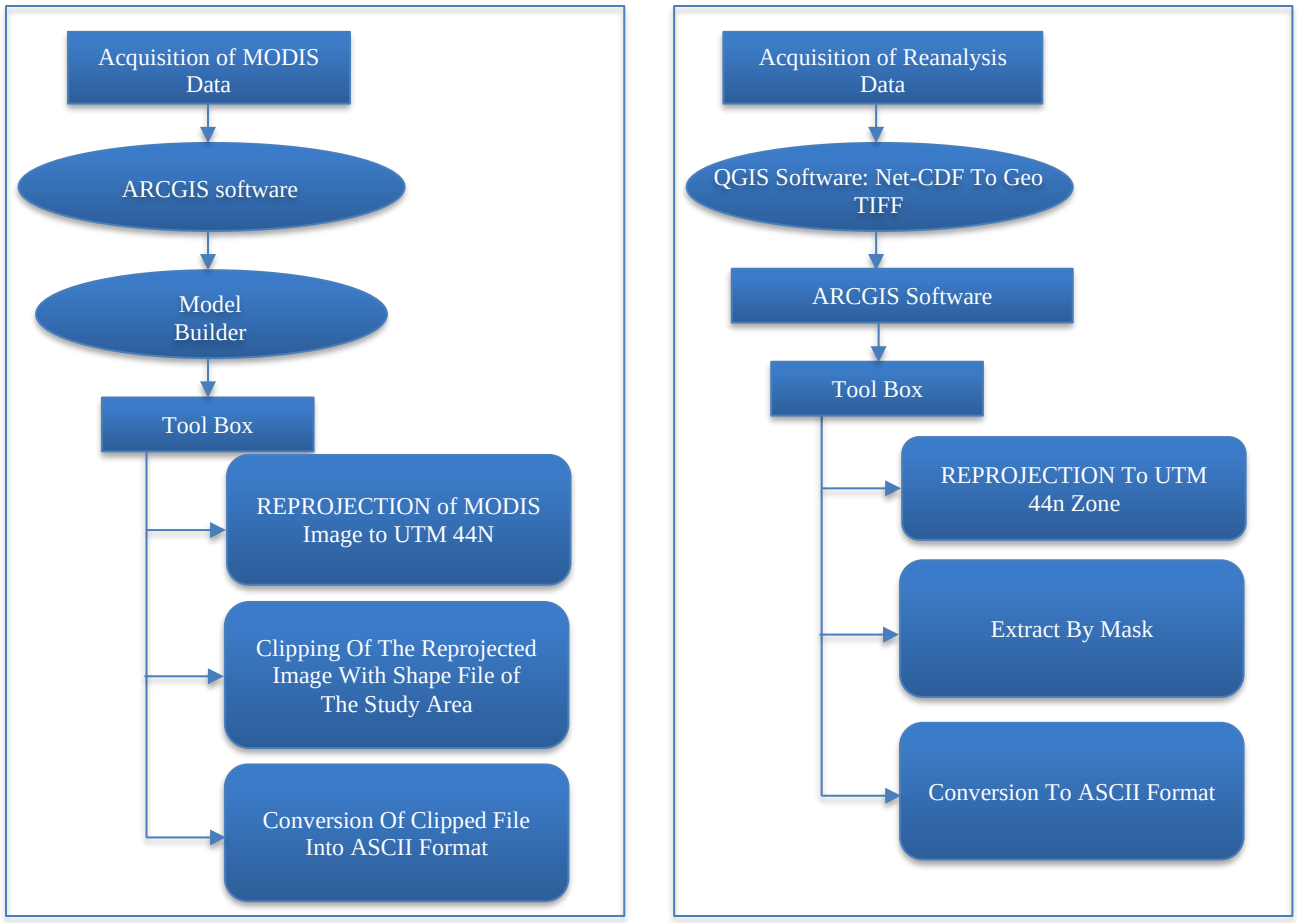

Fig. 2 Data preprocessing

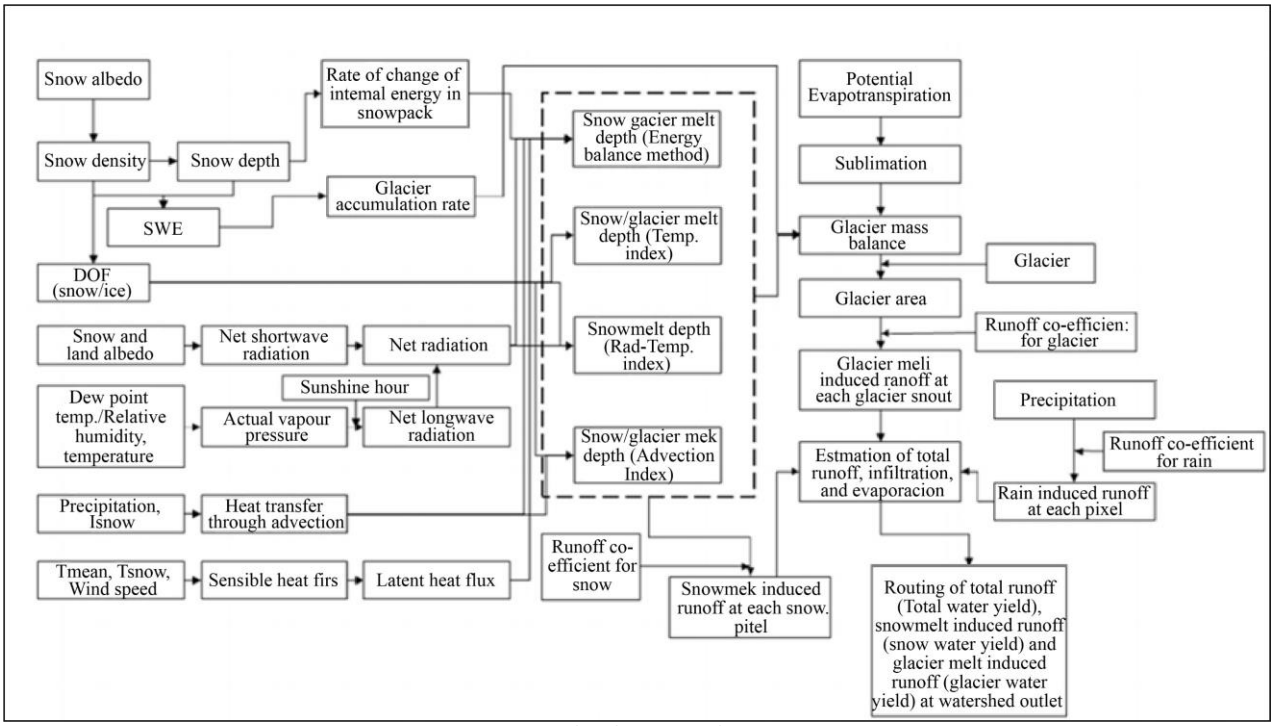

Fig. 3 Simplified flowchart of SDSGRM

Table 1. Details of acquired data

Data	Spatial resolution	Description	Source
i) Maximum temperature ii) Minimum temperature iii) Rainfall iv) iv)Daily discharge data	Point data	Observed	CWC
ASTER DEM	30 m	Static	NASA
LULC	100 m	Static	Copernicus Global Land service
Snow cover (MOD10A1) Snow Albedo (MOD10A1)	500 m	Optical	NSIDC
Surface albedo (MCD43A3)	500 m	Optical	LPDAAC
i) Snow layer temperature ii) 2m dew point temperature iii) 10m u component of wind iv) 10m v component of wind v) Max. relative humidity vi) Min. relative humidity vii) Min. temperature viii) Max. temperature ix) ix) Sunshine hour	0.25°	Reanalysis	ERA5

Table 2. Optimum calibration parameter value for the temperature index method

Sl. No	Parameter	Value Range	Optimum Value				
			2006-2007	2007-2008	2008-2009	2009-2010	Average
1.	Critical temperature	0-2	1.2	1.2	1.2	1.2	1.2
2.	Storage coefficient	0.04 - 0.08	0.04	0.04	0.04	0.04	0.04
3.	Runoff coefficient (rain)	0 - 1	0.5	0.5	0.5	0.5	0.5
4.	Runoff coefficient (snow melt)	0 - 1	0.8	0.7	0.7	0.8	0.75
5.	Melt factor for Ice temperature	1.3-2.6	2	2	2	2	2
6.	Melt factor for Ice radiation	0-0.1	0.025	0.025	0.025	0.025	0.025
7.	Sublimation factor (June 21)	0-1	0.5	0.5	0.5	0.5	0.5
8.	Sublimation factor (Dec 21)	0-1	0.4	0.4	0.4	0.4	0.4
9.	Basal coefficient	0.001-0.006	0.0015	0.0015	0.0015	0.0015	0.0015
10.	Ratio for meltwater refreezing	0-1	0.55	0.55	0.55	0.55	0.55
11.	Runoff coefficient (glacier)	0-1	0.009	0.01	0.01	0.009	0.009
12.	Runoff coefficient (rain)	0-1	0.009	0.01	0.01	0.009	0.009

Table 3. Optimum calibration parameter value for radiation-temperature index

Sl. No.	Parameter	Value Range	Optimum Value				
			2006-2007	2007-2008	2008-2009	2009-2010	Average
1.	Critical temperature	0-2	1.2	1.2	1.2	1.2	1.2
2.	Storage coefficient	0.04-0.08	0.04	0.04	0.04	0.04	0.04
3.	transmittance	0-0.1	0.099	0.099	0.099	0.099	0.099
4.	Sky view fraction	0.1-0.2	0.172	0.172	0.172	0.172	0.172
5.	Runoff coefficient (rain)	0 - 1	0.5	0.55	0.5	0.5	0.5
6.	Runoff coefficient (snow melt)	0 - 1	0.8	0.65	0.7	0.8	0.73
7.	Melt factor for Ice temperature	1.3-2.6	2	2	2	2	2
8.	Melt factor for Ice radiation	0-0.1	0.025	0.025	0.025	0.025	0.025
9.	Sublimation factor (June 21)	0-1	0.5	0.5	0.5	0.5	0.5
10.	Sublimation factor (December 21)	0-1	0.4	0.4	0.4	0.4	0.5
11.	Basal coefficient	0.001-0.006	0.0015	0.0015	0.0015	0.0015	0.0015
12.	Ratio for meltwater refreezing	0-1	0.98	0.98	0.95	0.98	0.97
13.	Runoff coefficient (glacier)	0-1	0.009	0.01	0.01	0.009	0.009
14.	Runoff coefficient (rain)	0-1	0.009	0.01	0.01	0.009	0.009

Table 4. Optimum calibration parameter value for advection-driven index

Sl. No	Parameter	Value Range	Optimum Value				
			2006-2007	2007-2008	2008-2009	2009-2010	Average
1.	Critical temperature	0-2	1.2	1.2	1.2	1.2	1.2
2.	Storage coefficient	0.04-0.08	0.04	0.04	0.04	0.04	0.04
3.	transmittance	0-0.1	0.099	0.099	0.099	0.099	0.099
4.	Sky view fraction	0.1-0.2	0.172	0.172	0.172	0.172	0.172
5.	Runoff coefficient (rain)	0 - 1	0.5	0.5	0.5	0.5	0.5
6.	Runoff coefficient (snow) melt	0 - 1	0.8	0.7	0.7	0.8	0.75
7.	Ice temperature melt factor	1.3 – 2.6	2	2	2	2	2
8.	Ice radiation melt factor	0 – 0.1	0.025	0.025	0.025	0.025	0.025
9.	Sublimation factor (June 21)	0-1	0.5	0.5	0.5	0.5	0.5
10.	Sublimation factor (Dec 21)	0-1	0.4	0.4	0.4	0.4	0.4
11.	Basal coefficient	0.001-0.006	0.0015	0.0015	0.0015	0.0015	0.0015
12.	Ratio for meltwater refreezing	0-1	0.92	0.95	0.94	0.92	0.93
13.	Runoff coefficient for glacier	0-1	0.006	0.01	0.01	0.006	0.008
14.	Runoff coefficient for rain	0-1	0.006	0.01	0.01	0.006	0.008

Table 5. Optimum calibration parameter value for energy balance method

Sl. No	Parameter	Value Range	Optimum Value				
			2006-2007	2007-2008	2008-2009	2009-2010	Average
1.	Critical temperature	0-2	1.2	1.2	1.2	1.2	1.2
2.	Storage coefficient	0.04-0.08	0.04	0.04	0.04	0.04	0.04
3.	Runoff coefficient (rain)	0 - 1	0.5	0.5	0.5	0.5	0.5
4.	Runoff coefficient (snow melt)	0 - 1	0.8	0.7	0.7	0.8	0.75
5.	Thermal quality (snow surface)	0.95-0.97	0.95	0.95	0.95	0.95	0.95
7.	Ice temperature melt factor	1.3-2.6	2	2	2	2	2
8.	Ice radiation melt factor	0-0.1	0.025	0.025	0.025	0.025	0.025
9.	Sublimation factor (June 21)	0-1	0.5	0.5	0.5	0.5	0.5
10.	Sublimation factor (December 21)	0-1	0.4	0.4	0.4	0.4	0.4
11.	Basal coefficient	0.001-0.006	0.0015	0.0015	0.0015	0.0015	0.0015
12.	Ratio for meltwater refreezing	0-1	0.95	0.95	0.96	0.95	0.95
13.	Runoff coefficient (glacier)	0-1	0.02	0.01	0.03	0.01	0.01
14.	Runoff coefficient (rain)	0-1	0.02	0.01	0.03	0.01	0.01

3. Result and Discussion

3.1. Model Assessment of SDSGRM

Calibration and validation were conducted to evaluate the SDSGRM using the temperature-based index method, radiation-temperature index technique, advection-driven index approach, and an enhanced energy balance approach. Each method was calibrated separately, with parameters adjusted accordingly.

The best-fit values were determined for each calibration period, and validation of the model was performed for the timeframe from October 2012 to October 2013 and March 2014 to November 2014. Figure 4 presents the temporal variations in runoff and precipitation, facilitating a comparative assessment of each method's precision.

Among the tested approaches, the energy balance method demonstrates the most consistent accuracy in estimating runoff during both calibration and validation periods. Previous studies have highlighted that energy balance models perform effectively in high-altitude glaciated environments [19]. The influence of precipitation is evident, with higher rainfall generally leading to increased runoff across all methods.

However, peak flow events are often overestimated, particularly during intense precipitation periods. Some instances of overprediction and underprediction are noted, likely attributable to variabilities in model assumptions and probable variations in observed data [20].

The statistical assessment of SDSGRM, outlined in Table 6, highlights key performance indicators across methods. R^2 values vary between 0.61 and 0.78, with the energy balance method consistently achieving the highest values, indicating a robust model fit.

However, ME values fluctuate, with the energy balance method showing the highest ME, suggesting a tendency toward flow overestimation. Nevertheless, ME remains near zero for all methods, signifying relatively accurate

predictions. CRM values range from -0.16 to 0.22, reflecting varying biases across different approaches. The energy balance method demonstrates minimal bias, as indicated by CRM values close to zero, while other methods exhibit a broader range of CRM values, indicating higher potential bias in certain cases. During validation, ME values increase slightly (0.57 to 0.65), with the energy balance method maintaining a relatively high ME, reinforcing its overestimation tendency. However, all methods continue to display ME values near zero, signifying acceptable accuracy. R^2 values range between 0.63 and 0.67, reaffirming strong predictive performance, with the energy balance method again ranking highest. CRM values during validation (0.11 to 0.19) remain consistent with calibration results, indicating minor but persistent biases. The energy balance method retains relatively low CRM values, reinforcing its stability and reliability. Overall, the SDSGRM demonstrates acceptable efficiency, with the energy balance method emerging as the most effective approach based on key indicators, including R^2 and CRM.

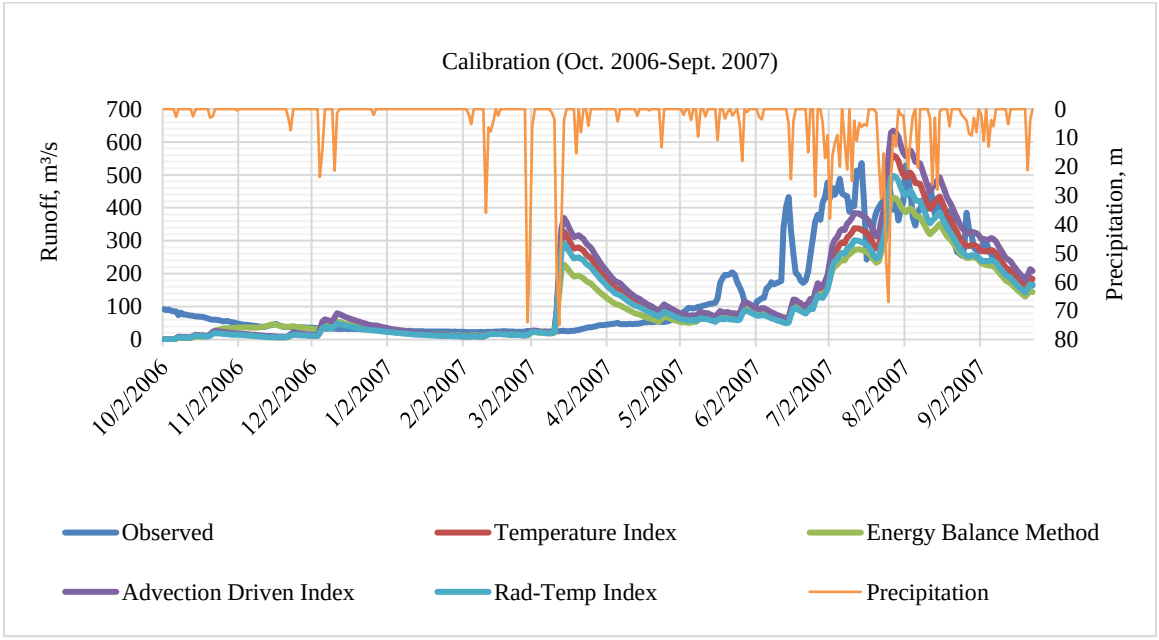

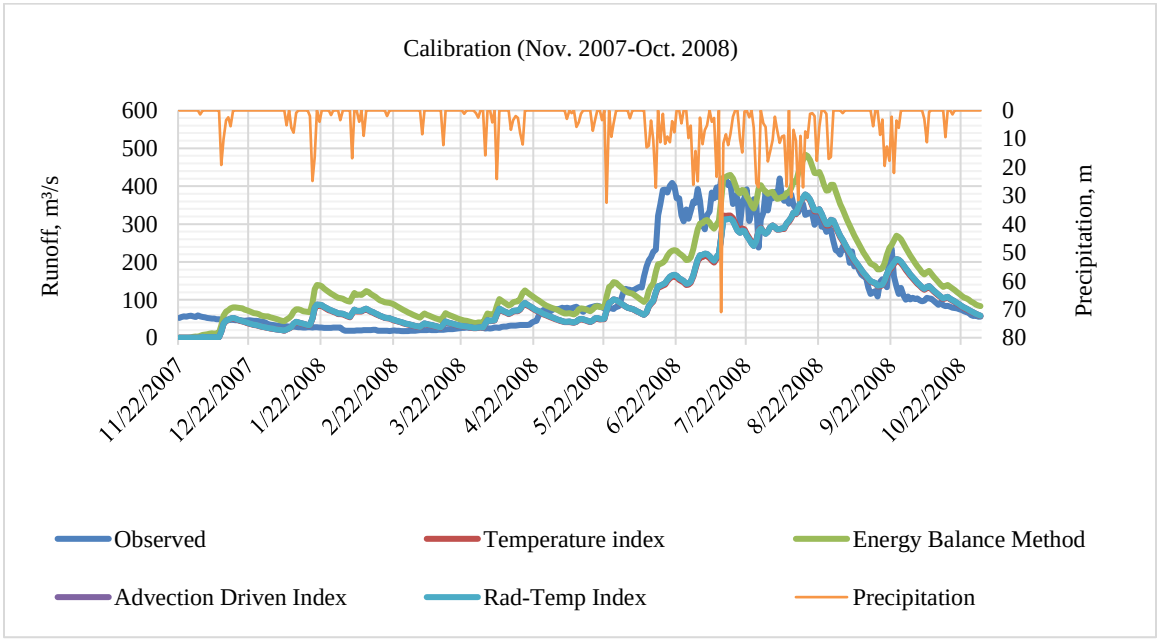

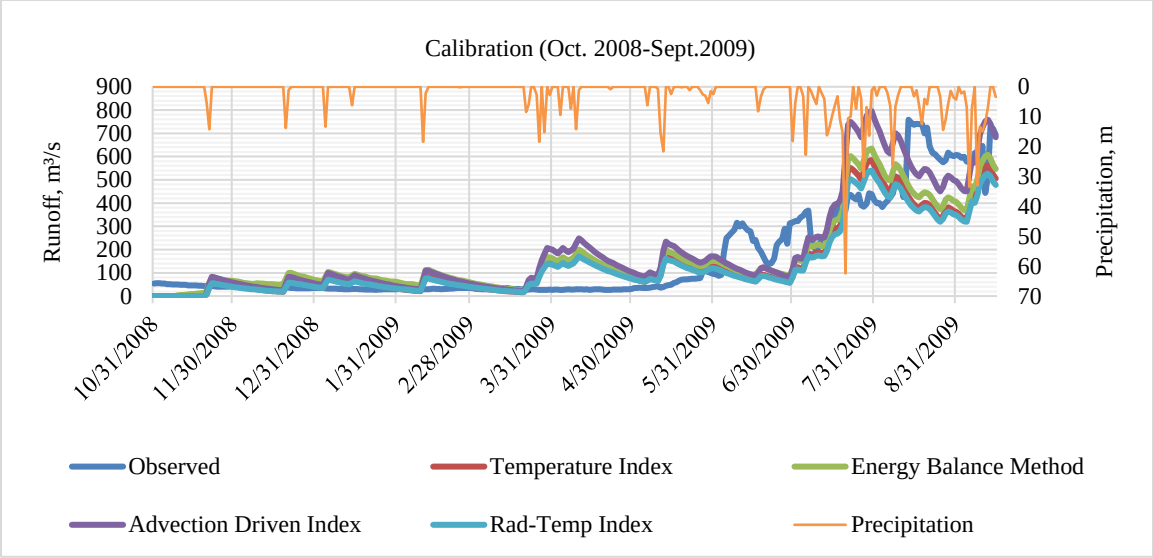
Calibration (Oct. 2008-Sept.2009)
Runoff, m³/s
Precipitation, m
900
800
700
600
500
400
300
200
100
0
0
10
20
30
40
50
60
70
10/31/2008
11/30/2008
12/31/2008
1/31/2009
2/28/2009
3/31/2009
4/30/2009
5/31/2009
6/30/2009
7/31/2009
8/31/2009
Observed
Temperature Index
Energy Balance Method
Advection Driven Index
Rad-Temp Index
Precipitation

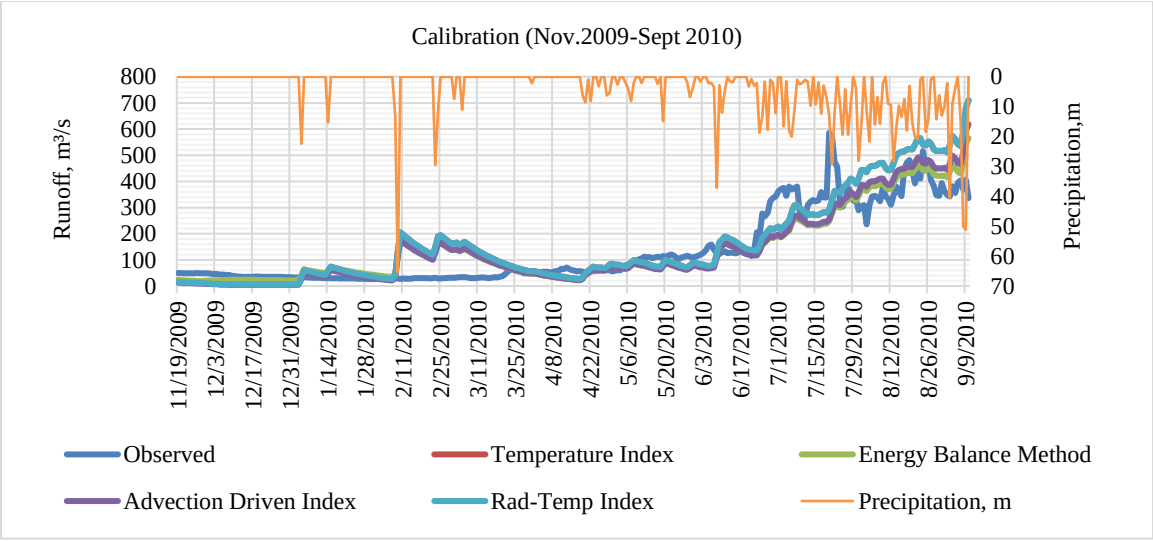
Calibration (Nov.2009-Sept 2010)
Runoff, m³/s
Precipitation,m
800
700
600
500
400
300
200
100
0
0
10
20
30
40
50
60
70
11/19/2009
12/3/2009
12/17/2009
12/31/2009
1/14/2010
1/28/2010
2/11/2010
2/25/2010
3/11/2010
3/25/2010
4/8/2010
4/22/2010
5/6/2010
5/20/2010
6/3/2010
6/17/2010
7/1/2010
7/15/2010
7/29/2010
8/12/2010
8/26/2010
9/9/2010
Observed
Temperature Index
Energy Balance Method
Advection Driven Index
Rad-Temp Index
Precipitation, m

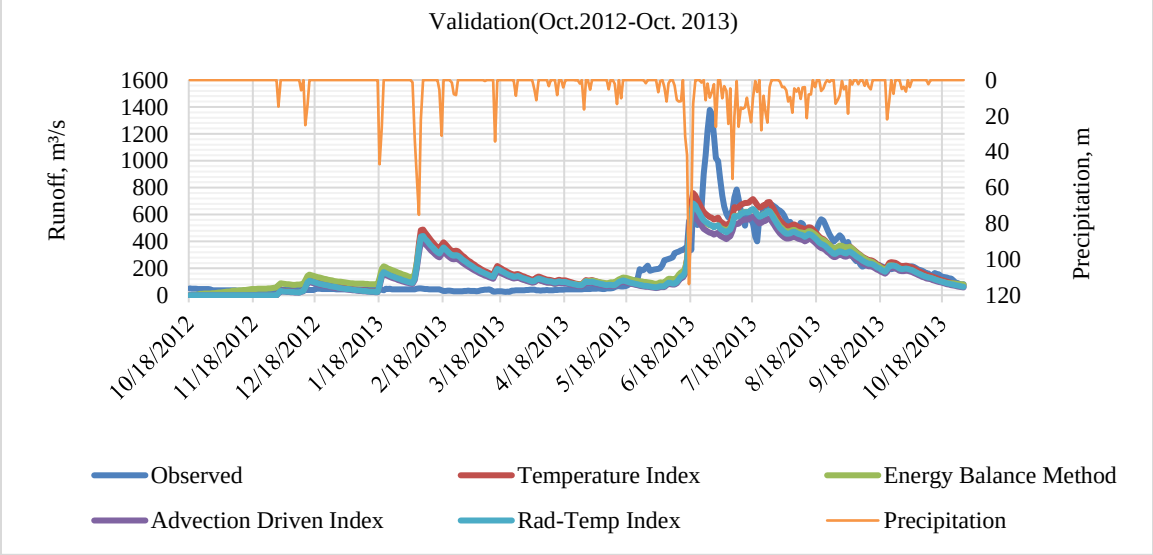
Validation(Oct.2012-Oct. 2013)
Runoff, m³/s
Precipitation, m
1600
1400
1200
1000
800
600
400
200
0
0
20
40
60
80
100
120
10/18/2012
11/18/2012
12/18/2012
1/18/2013
2/18/2013
3/18/2013
4/18/2013
5/18/2013
6/18/2013
7/18/2013
8/18/2013
9/18/2013
10/18/2013
Observed
Temperature Index
Energy Balance Method
Advection Driven Index
Rad-Temp Index
Precipitation

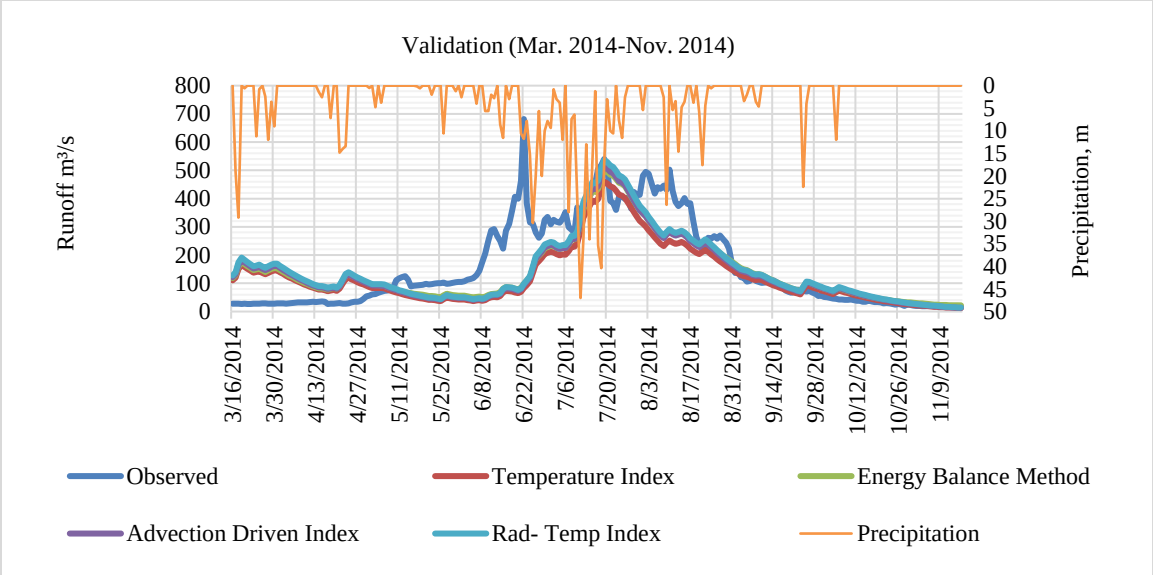

Fig. 4 Temporal trend analysis using the temperature index method, radiation temperature index method, advection-driven index method, and energy balance approach

Table 6. Statistical performance of SDSGRM

Calibration	Temperature Index Method				Radiation-Temperature Index				Advection Driven Index				Energy Balance Method			
	2006-2007	2007-2008	2008-2009	2009-2010	2006-2007	2007-2008	2008-2009	2009-2010	2006-2007	2007-2008	2008-2009	2009-2010	2006-2007	2007-2008	2008-2009	2009-2010
ME	0.57	0.71	0.70	0.65	0.58	0.72	0.69	0.64	0.51	0.72	0.65	0.79	0.62	0.70	0.72	0.77
R^2	0.61	0.74	0.71	0.77	0.61	0.74	0.72	0.77	0.61	0.74	0.71	0.77	0.68	0.76	0.72	0.78
CRM	0.09	0.13	0.11	-0.16	0.19	0.12	0.16	-0.16	-0.04	0.12	0.19	-0.01	0.22	0.22	-0.03	-0.01
SEE	94.30	68.02	112.6	84.54	93.95	67.70	114.2	84.54	100.4	67.78	121	71.22	87.73	70.26	108	67.83
Validation	**Temperature Index Method**		**Radiation-Temperature Index**		**Advection Driven Index**		**Energy Balance Method**									
	2012-2013	2013-2014	2012-2013	2013-2014	2012-2013	2013-2014	2012-2013	2014								
ME	0.64	0.57	0.64	0.60	0.62	0.61	0.65	0.62								
R^2	0.65	0.65	0.65	0.63	0.64	0.65	0.67	0.66								
CRM	-0.11	-0.08	0	-0.09	0.09	0.19	-0.08	0.17								
SEE	146.28	101.33	145.50	98.78	149.72	97.75	143.44	96.11								

Despite its effectiveness, the model exhibits occasional limitations in efficiency metrics, particularly lower ME and R^2 values in some instances, are likely due to uncertainties in input data, model assumptions, and climatic variability [21]. Similar efficiency metrics have been observed in previous studies.

Figure 5 illustrates the scatter plot of the calibrated and validation periods. Satellite-derived and reanalysis datasets are crucial for evaluating snow and glacier melt but pose inherent challenges. Cloud cover complicates the applicability of MODIS snow cover and albedo data (MCD43A3), often reducing data reliability during monsoon months [22].

Additionally, the deposition of dust and the presence of black carbon lead to variations in snow albedo and introduce inaccuracies in melt rate estimations [23-25]. ERA5 reanalysis data, despite being widely utilized, relies on model interpolations that may not accurately capture localized temperature, precipitation, and wind variations in glacierized regions [26, 27]. The scarcity of in-situ observations further complicates the validation of satellite-derived datasets, particularly in remote basins like Alaknanda. Addressing these challenges requires integrating multiple data sources, applying regional bias corrections, and refining snow and albedo calibration techniques to enhance model accuracy [28].

3.2. Assessment of Runoff and Variability in SMY, GMY and RWY

SDSGRM was employed to analyze the variability in streamflow contributions from precipitation-induced runoff, snowmelt, and glacier melt. The proportionate contributions of Rain Water Yield (RWY), Snow Water Yield (SWY), and Glacier Water Yield (GWY), evaluated using the radiation-temperature index technique and the energy balance approach, exhibited similar trends, as summarized in Table 7.

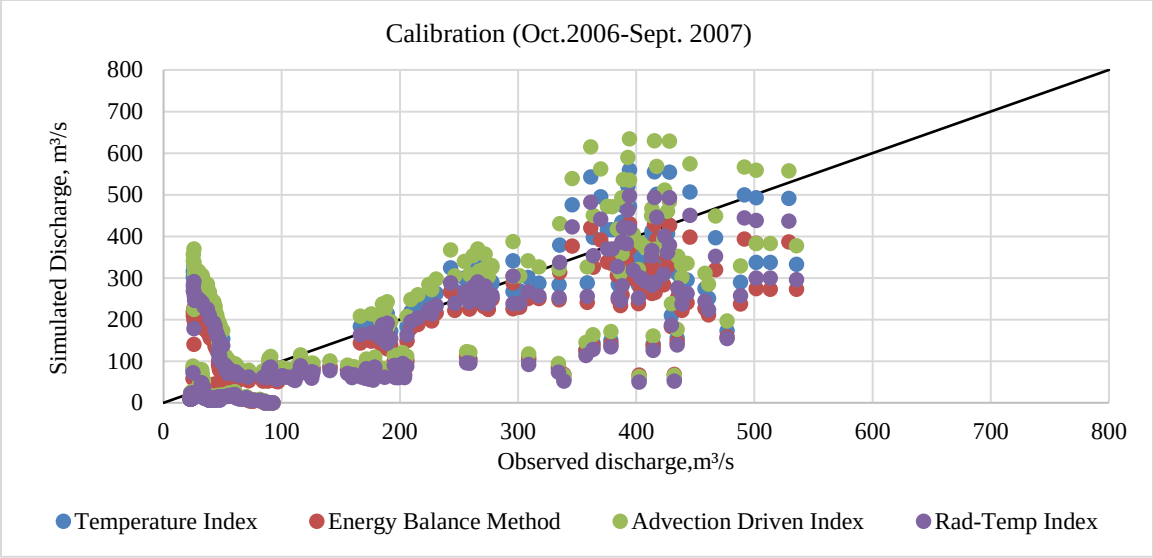
Calibration (Oct.2006-Sept. 2007)
Simulated Discharge, m³/s
Observed discharge,m³/s
0
100
200
300
400
500
600
700
800
Temperature Index
Energy Balance Method
Advection Driven Index
Rad-Temp Index

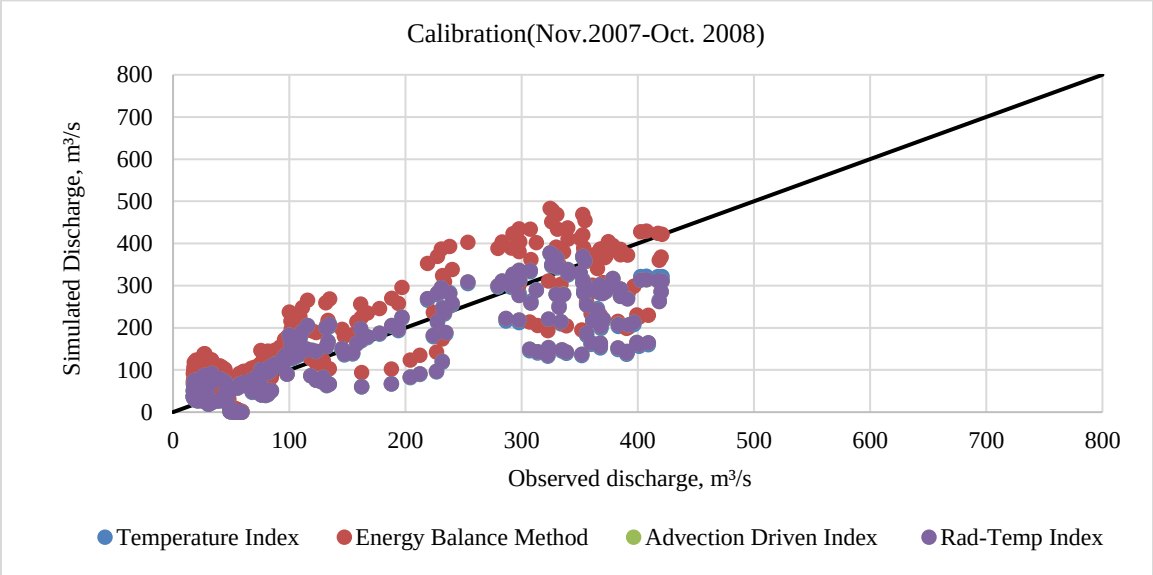
Calibration(Nov.2007-Oct. 2008)
Simulated Discharge, m³/s
Observed discharge, m³/s
0
100
200
300
400
500
600
700
800
Temperature Index
Energy Balance Method
Advection Driven Index
Rad-Temp Index

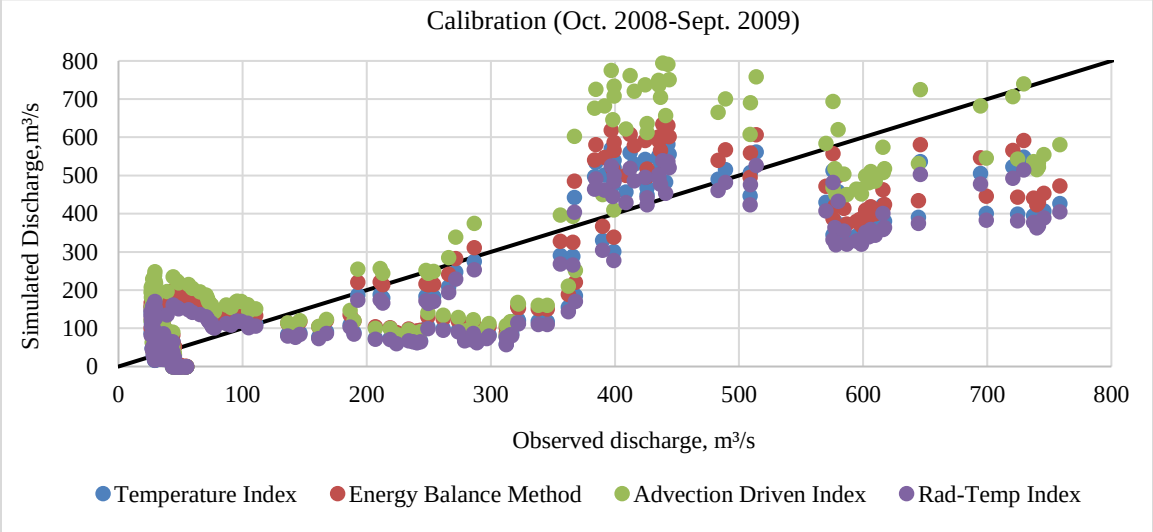
Calibration (Oct. 2008-Sept. 2009)
Simulated Discharge,m³/s
Observed discharge, m³/s
0
100
200
300
400
500
600
700
800
Temperature Index
Energy Balance Method
Advection Driven Index
Rad-Temp Index

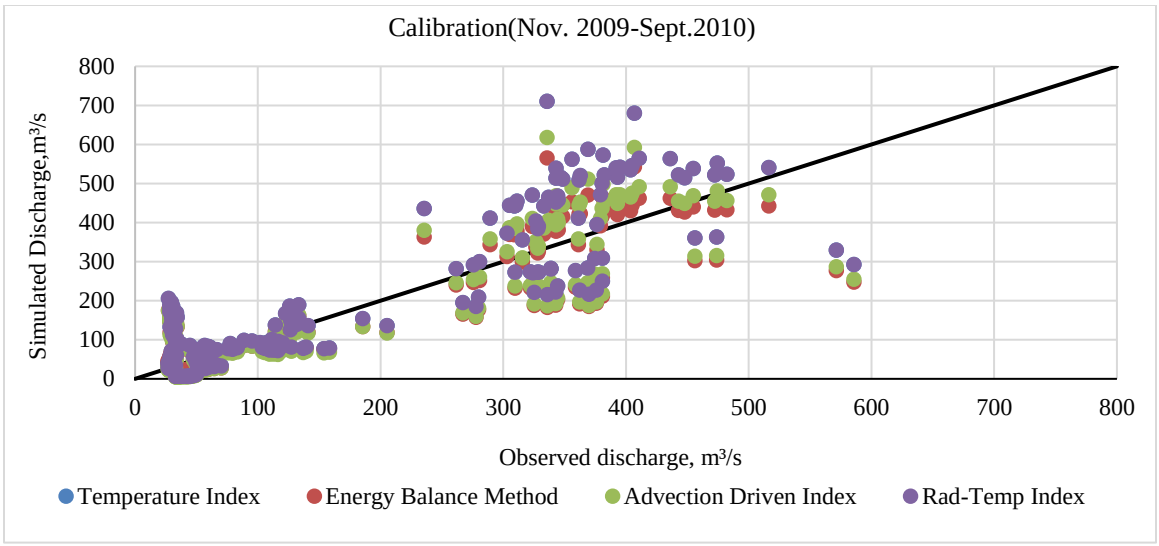

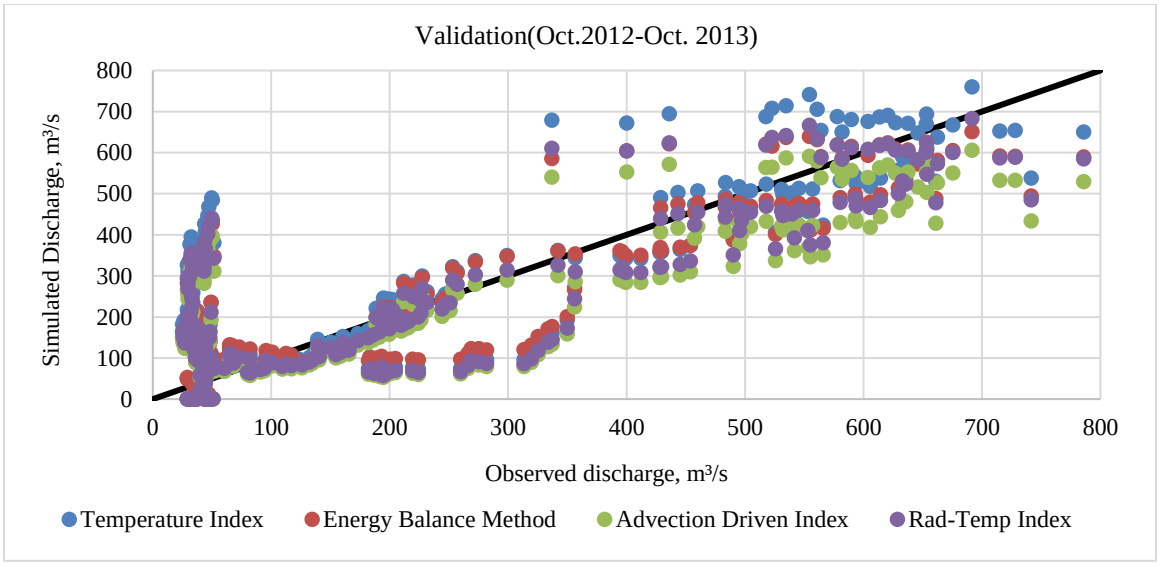

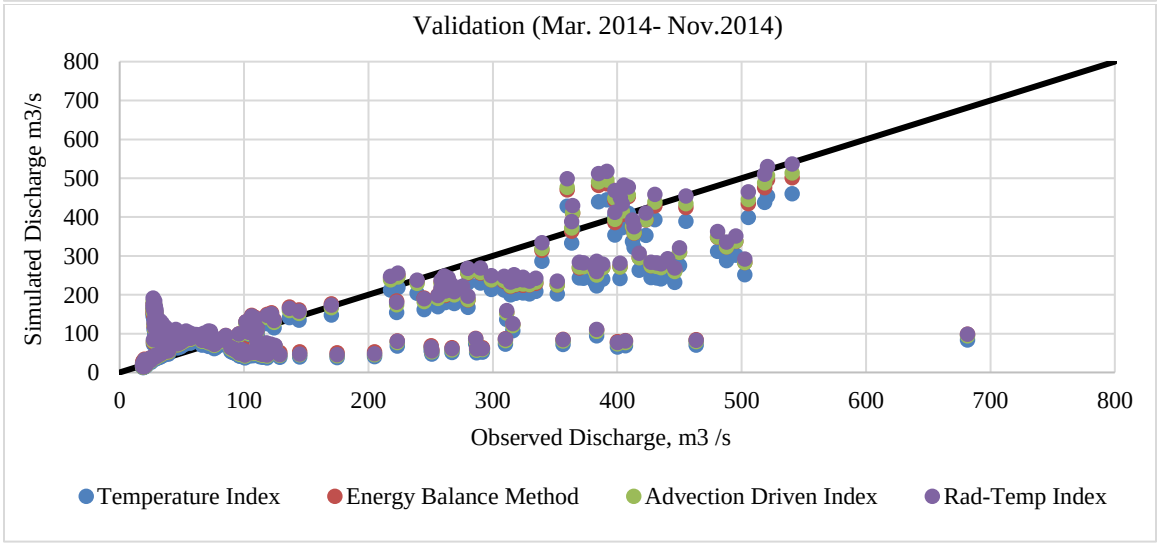

Fig. 5 Graphical scatter analysis for the temperature index method, radiation temperature index method, advection-driven index method, and energy balance approach

Table 7. Runoff composition in terms of percentage from snowmelt, glacier melt, and precipitation-induced flow

Method	Calibration											
	2006-2007			2007-2008			2008-2009			2009-2010		
	RWY	SWY	GWY	RWY	SWY	GWY	RWY	SWY	GWY	RWY	SWY	GWY
Radiation-Temperature Index	89.97	9.92	0.10	97.65	2.22	0.12	93.6	6.12	0.25	91.47	8.33	0.18
Energy Balance Method	89.96	9.91	0.10	99.34	0.48	0.17	92	7.2	0.3	90.33	9.58	0.07
Method	**Validation**					
	2012-2013			2013-2014		
	RWY	SWY	GWY	RWY	SWY	GWY
Radiation-Temperature Index	90.80	9.03	0.17	94.60	5.10	0.18
Energy Balance Method	89.93	9.85	0.21	98.67	1.18	0.14

Figure 6 and Figure 7 illustrate the contributions of RWY, SWY, and GWY. Variability in runoff contributions from SWY, GWY, and RWY was assessed across both calibration and validation periods. Under the radiation-temperature index approach, SWY fluctuated between 2.22% and 9.92% across different years. The highest SWY contribution was recorded in 2006–2007, while the lowest occurred in 2007–2008, illustrating that snowmelt's role in runoff generation is highly dependent on seasonal and interannual climatic variations [29, 30]. Conversely, GWY remained relatively low, ranging between 0.10% and 0.25%.

RWY emerged as the dominant component, accounting for 89.97% to 97.65% of total runoff, reaffirming that rainfall is the primary driver of streamflow. When analyzed using the energy balance method, SWY showed a broader range, fluctuating between 0.48% and 9.91%. A notable decline in snowmelt contribution was observed in 2007–2008, which may reflect changing snowpack conditions or calibration inconsistencies.

GWY remained low, ranging from 0.07% to 0.30%, highlighting the consistent but limited role of glacier melt in overall runoff. RWY continued to be the predominant source, ranging between 89.96% and 99.34%, confirming that rainfall remains the primary driver of runoff in the basin. During the validation period, runoff contributions followed similar patterns.

SWY under the radiation-temperature index method ranged from 5.10% to 9.03%, showing a slight reduction from the calibration phase, though it remained a significant factor in runoff formation. GWY exhibited minor fluctuations, increasing slightly from 0.17% to 0.18%, reaffirming its minimal contribution to total streamflow. RWY maintained its dominance, ranging from 90.80% to 94.60%, further supporting the conclusion that rainfall is the main source of runoff generation. Throughout the validation phase, the energy balance method revealed fluctuations in SWY, ranging between 9.85% and 1.18%, with a notable drop in 2013–2014.

This decline may indicate high interannual variability or potential calibration inconsistencies. GWY exhibited relatively stable values, remaining between 0.14% and 0.21%, reaffirming its minimal role in overall streamflow. In contrast, RWY consistently dominated, contributing between 89.93% and 98.67%, highlighting precipitation as the primary factor influencing total runoff within the basin.

Throughout both calibration and validation periods, RWY gradually increased from May through October, reaching its peak in either July or August, depending on annual rainfall variations [17]. The prominence of RWY as the dominant driver of runoff generation aligns with previous findings [31] since the summer monsoon season (May to October) contributes more than 80% of the annual precipitation. In the Greater Himalayan region [32].

In contrast, both SWY and GWY peaked before the onset of the monsoon, gradually declining as the season progressed [33]. Observations indicate that GWY maintained a consistent yet limited role in overall runoff generation. This suggests that although the total amount of snowmelt and glacial melt remains largely unchanged, their share of total runoff fluctuates in response to variations in rainfall-driven runoff [34].

3.3 Comparison Between Glacier Area Estimates Derived from the Automated Glacier Extraction Index (AGEI)

SDSGRM incorporates a glacier area computation tool that determines daily glacier area throughout the snow period using an input glacier map from a single reference year.

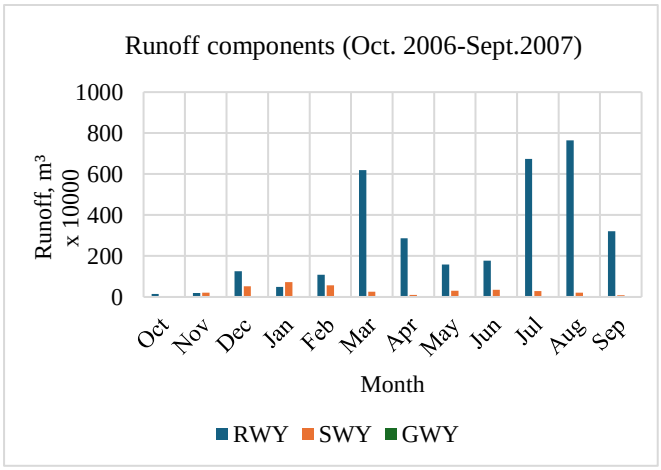

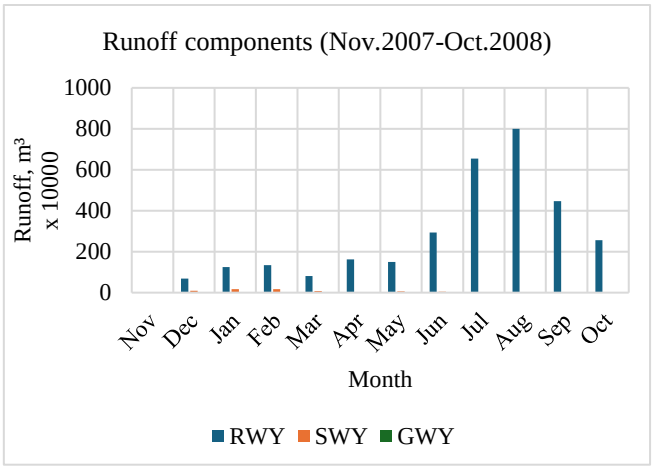

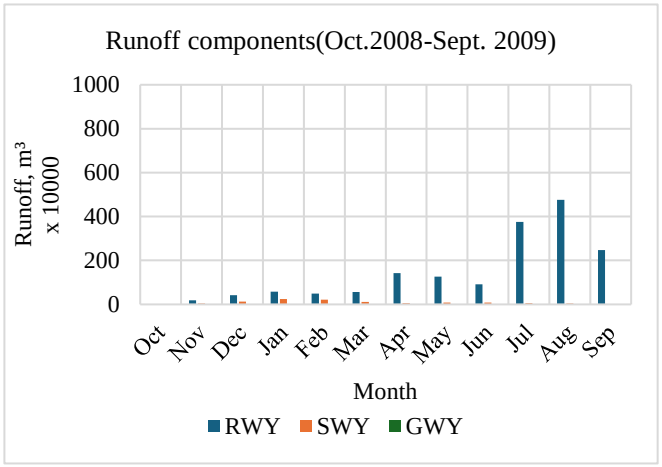

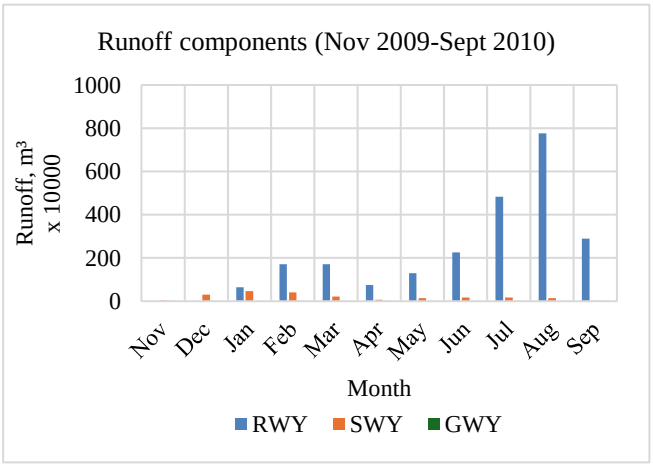

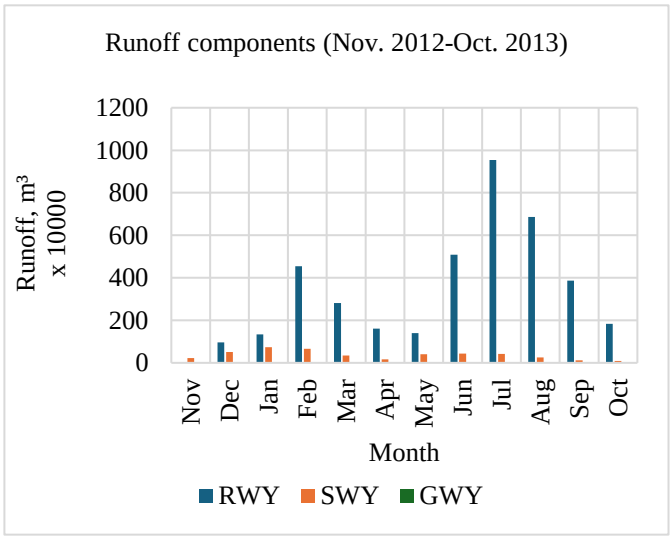

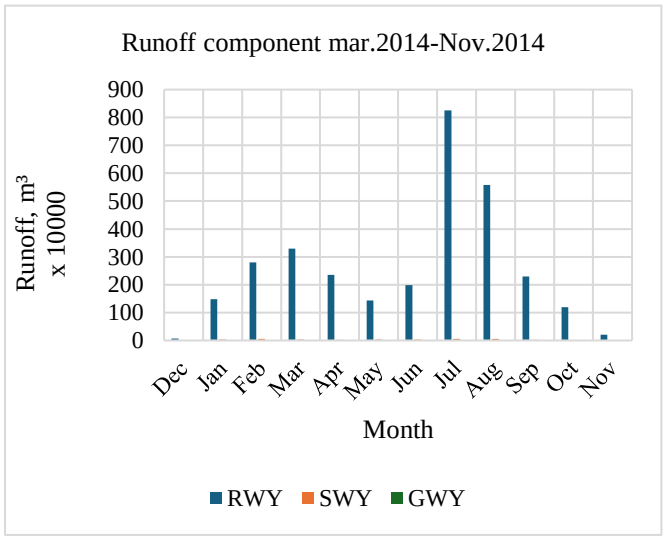

Fig. 6 Runoff components generated using energy balance method for calibration year

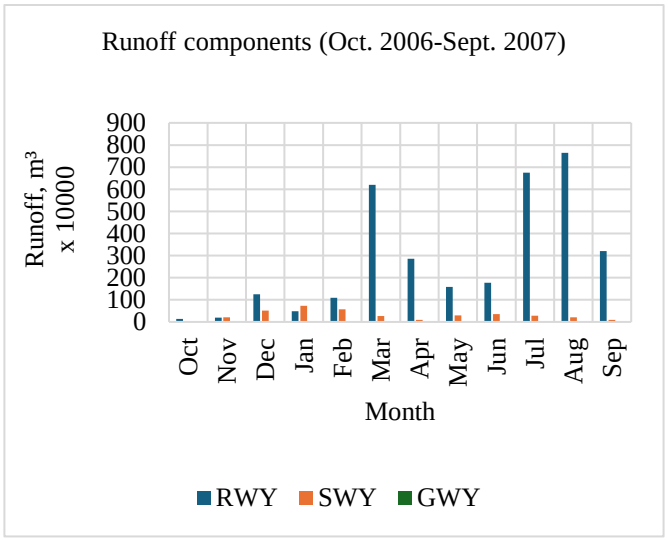

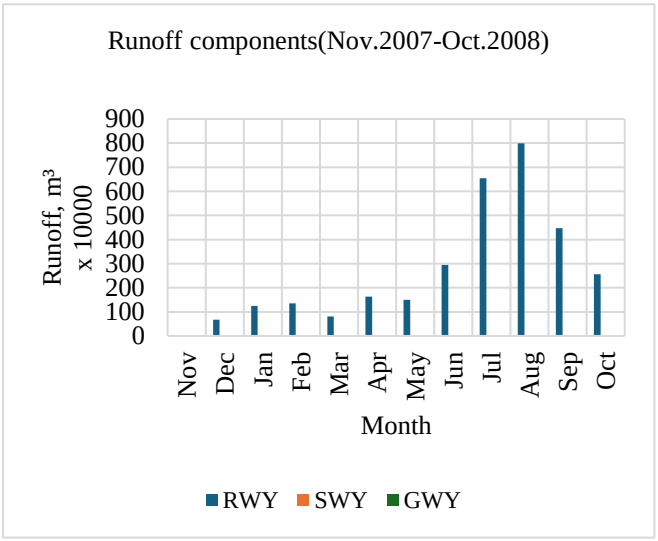

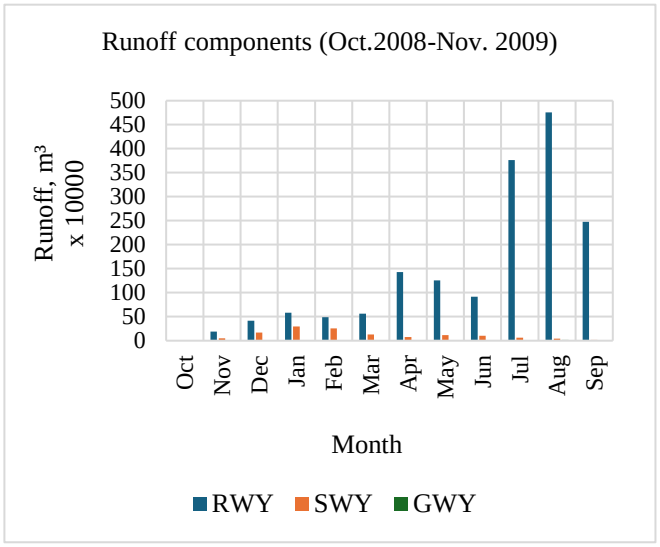

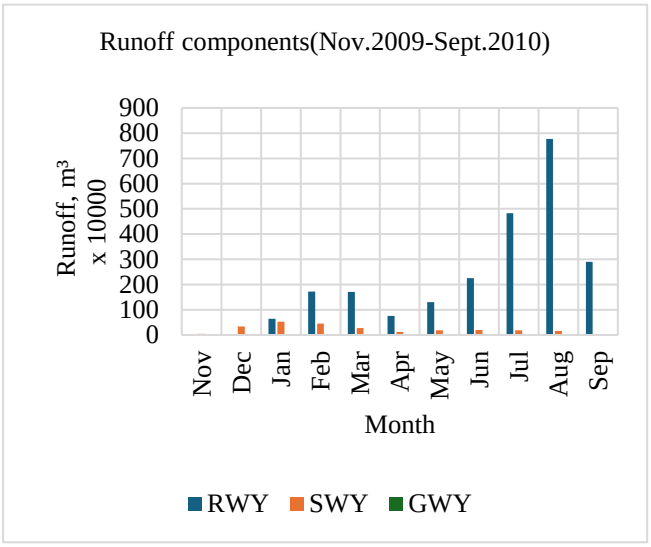

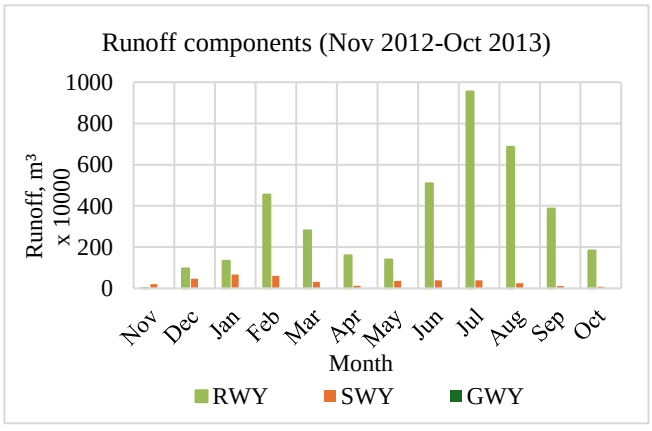

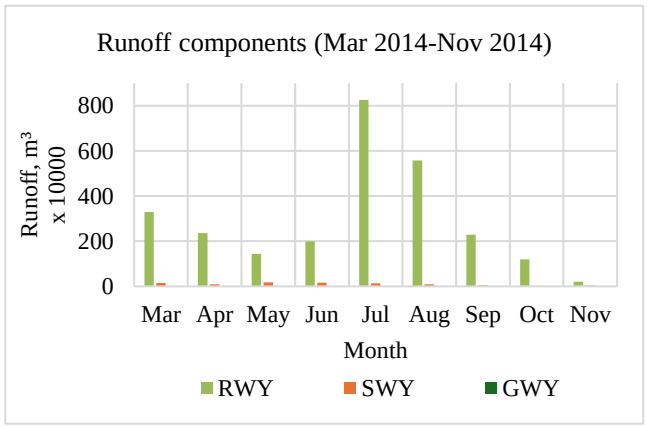

Fig. 7 Runoff components generated using energy balance method for validation year

This method enables the model to integrate daily glacier area data to estimate glacier melt runoff while also considering other hydrological parameters. Table 8 presents a comparison between glacier area estimates obtained from the Automated Glacier Extraction Index (AGEI) [35] and those derived using the energy balance method.

Table 8. Comparison of glacier area (km²) generated from automated glacier extraction index and glacier area derived from snowmelt generated using the energy balance method

Year	AGEI	Energy Balance Method
2006-2007	1034.07	1001.88
2007-2008	1071.36	858.35
2008-2009	1102.20	1081.88
2009-2010	1052.80	1079.10
2012-2013	918.14	922.42
2014	877.07	903.63
Avg. Difference		34.73
% Difference		3.14

This multi-year comparison assesses the consistency of both approaches in estimating glacier areas. Results indicate that glacier area estimates from AGEI and the energy balance method closely align, with a mean variation of 34.73 km² and a percentage variation of 3.14%. This close agreement validates the model's reliability in estimating glacier area and the corresponding runoff.

3.4. Spatio-Temporal Variations in Snow and Glacial Parameters

The temporal plot of pixel average values for various parameters is depicted in Figure 8. The average values for snow parameters provide insight into seasonal variations in snowpack characteristics, indicating that the Degree Day Factor (DDF), snow density, and snow depth for both snow and glaciers tend to be higher during summer months (June to August), while lower values are observed in winter due to temperature fluctuations and melting processes. Snow density was found to be greater during months with wet snow, while colder months (with dry snow) exhibited lower values. Across different study periods, snow density has averaged around 450 kg/m³, fluctuating between 350 kg/m³ and 500 kg/m³ depending on the season [36]. The average Snow Water Equivalent (SWE) typically varies between 0.7 m and 2.6 m, significantly influencing runoff patterns.

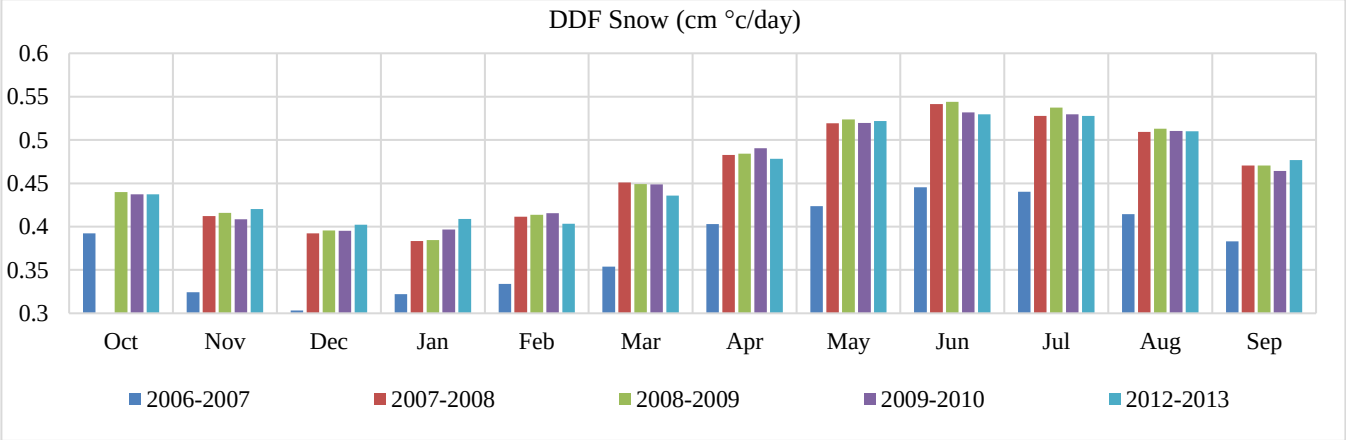

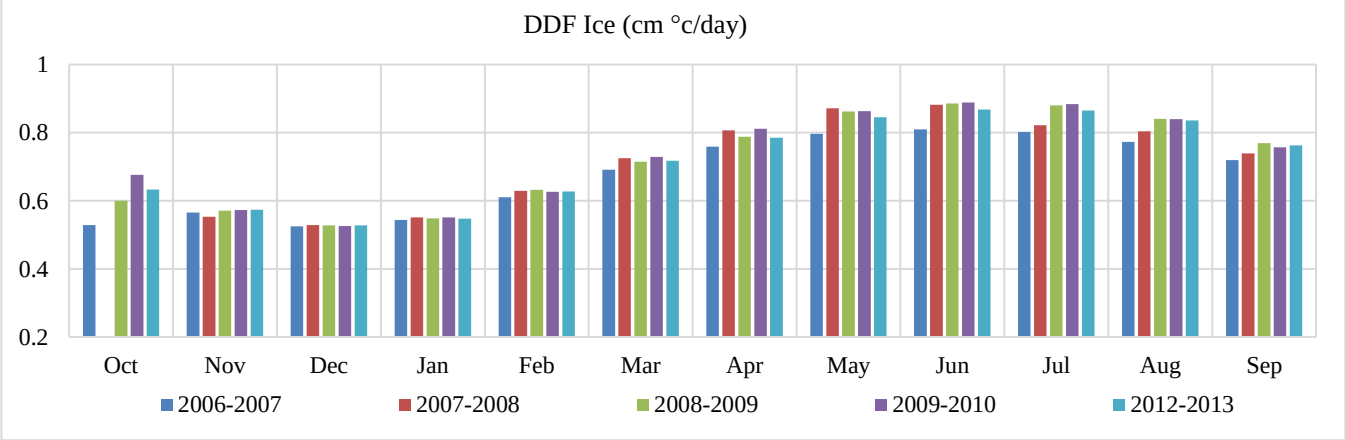

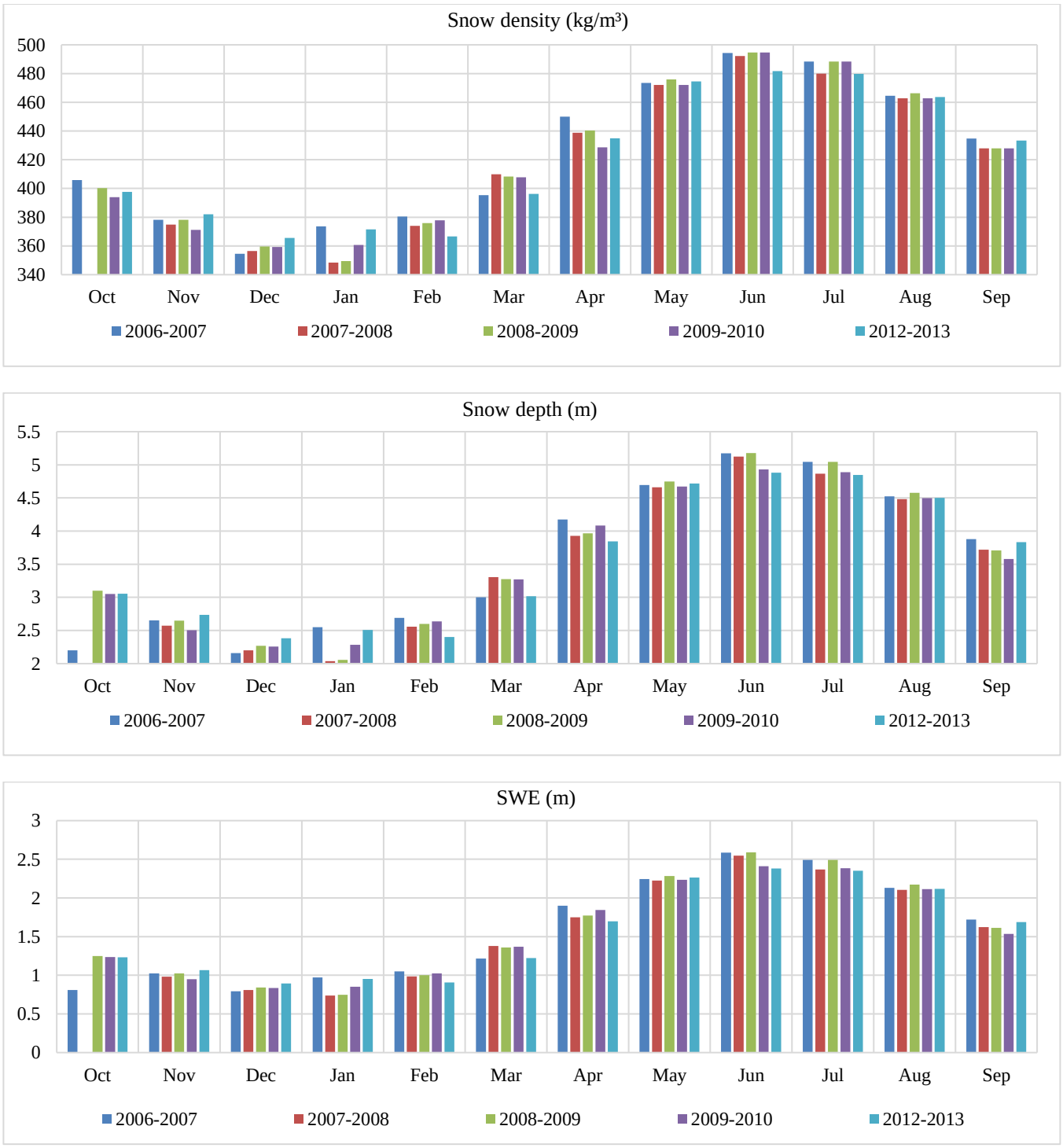

Fig. 8 Time series plot of different snow parameters

The mean DDF for snow ranges between 0.30 cm/°C/day and 0.54 cm/°C/day, while glacier DDF values vary between 0.52 cm/°C/day and 0.91 cm/°C/day, reflecting the different melting rates of snow and ice surfaces. Snow depth fluctuates throughout the year, averaging 3.5 m, and typically peaks from May to August before declining with the onset of winter.

These variations highlight the dynamics of snow and glacier parameters within high-altitude basins. Changes in snow density, SWE, and DDF directly impact runoff contributions. Figure 9 shows the spatial monthly average for the following parameters: sensible heat flux, latent heat flux, snow DDF, snow density, and snow depth.

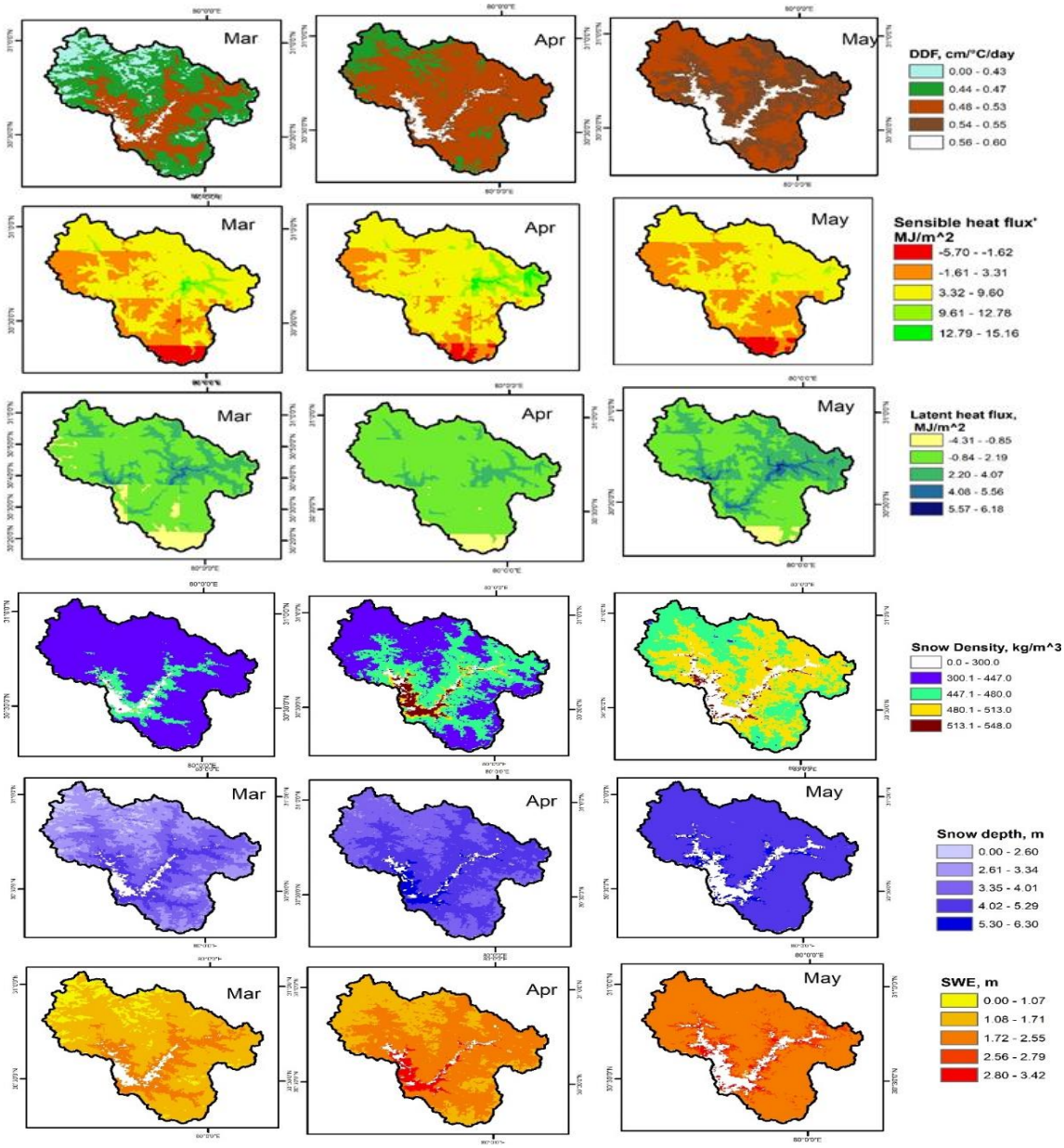

Fig. 9 Monthly average SDSGRM generated snow parameter outputs

3.5. Climate Change Implication on Water Resource

The lower reaches of Himalayan rivers heavily depend on streamflow, making hydrological resource monitoring imperative in the Alaknanda River Basin and other high-altitude regions crucial, particularly in focus on climate change. Climate change has significantly influenced irrigation patterns and cropping intensity [37]. Given the dominance of rainfall-driven runoff, policymakers and water resource managers should prioritize sustainable watershed management practices that enhance precipitation capture and storage [7].

Climate change has exacerbated the region's hydrologic imbalance, with rising temperatures accelerating glacier retreat and altering snowmelt patterns. This may lead to increased short-term runoff, followed by long-term water shortages [38]. In the High Mountain Asia region, including major river systems like the Ganges, Brahmaputra, and Indus, meltwater serves as a critical source of downstream water supply. Research indicates that while the western part of this region relies heavily on meltwater during the summer dry season, the eastern regions are dominated by monsoon-driven runoff. This underscores the need for tailored water management strategies that consider distinct seasonal melt patterns [1].

Additionally, the Alaknanda River Basin is highly susceptible to Glacial Lake Outburst Floods (GLOFs).

Comprehensive evaluations of glacial lakes have identified potential hazards, emphasizing the importance of continuous monitoring and risk reduction measures [39].

Adaptive water management strategies require real-time tracking of snowpack dynamics and meltwater contributions. The incorporation of remote sensing and ground-based data has substantially refined the accuracy of snowmelt and water resource predictions. Long-term data acquisition is essential for understanding trends and fluctuations, enabling the development of responsive water allocation policies that adapt to shifting meltwater patterns [40]. Incorporating SDSGRM into water resource planning can support adaptive management by providing reliable runoff simulations essential for optimizing reservoir storage, mitigating flood risks, and enhancing climate resilience. Furthermore, combining SDSGRM with advanced climate models and real-time remote sensing could further refine predictions, enabling proactive climate adaptation strategies.

4. Conclusion

This study evaluated the performance of SDSGRM in simulating runoff within a glaciated basin. Across both calibration and validation periods, all tested methods demonstrated satisfactory results, reinforcing the model's reliability for hydrological assessments and climate impact studies. Among these methods, the energy balance approach consistently outperformed the others, delivering the most accurate runoff estimations.

The findings confirmed that rainfall is the dominant driver of streamflow generation, contributing over 89% to total runoff. Snow Water Yield (SWY) exhibited seasonal variations, peaking before the monsoon, whereas Glacier Water Yield (GWY) remained a minor yet stable contributor. These results align with previous research, underscoring the central role of precipitation in high-altitude hydrology. Additionally, glacier area estimates from the Automated Glacier Extraction Index (AGEI) were compared with SDSGRM outputs, revealing an average discrepancy of just 3.14%, further validating the model's accuracy.

Seasonal variations in snow and glacier parameters followed expected trends, with higher snow density and depth recorded during summer (May-August) and lower values observed in winter. Integrating SDSGRM with remote sensing and real-time data assimilation could enhance water resource forecasting and support proactive climate adaptation strategies. Future studies could further refine the model by incorporating advanced climate projections and high-resolution observational datasets, ensuring more precise hydrological predictions in glacierized basins.

Funding Statement

The authors gratefully acknowledge the help, encouragement and financial support provided by the Climate Change Programme (CCP), Strategic Programmes, Large Initiatives and Coordinated Action Enabler (SPLICE), Department of Science and Technology, Govt. of India under National Mission on Sustaining Himalayan Ecosystem (NMSHE) through Grant No. DST/CCP/MRDP/184/2019.

Acknowledgement

The authors would like to acknowledge and sincerely thank the organizing committee of the International Conference on Computer-Aided Modeling for the Sustainable Development of Smart Cities (CAMSSC), sponsored by the Anusandhan National Research Foundation (ANRF), held at the Department of Civil Engineering, North Easstern Regional Institute of Science and Technology (NERIST), Nirjuli, Arunachal Pradesh, India, during November 27–30, 2024, for allowing us to present the paper and sponsoring the paper for publication.

References

[1] Richard L. Armstrong et al., "Runoff from Glacier Ice and Seasonal Snow in High Asia: Separating Melt Water Sources in River Flow," *Regional Environmental Change*, vol. 19, pp. 1249-1261, 2019. [CrossRef] [Google Scholar] [Publisher Link]

[2] G. Jeelani et al., "Role of Snow and Glacier Melt in Controlling River Hydrology in Liddar Watershed (Western Himalaya) under Current and Future Climate," *Water Resources Research*, vol. 48, no. 12, pp. 1-16, 2012. [CrossRef] [Google Scholar] [Publisher Link]

[3] Peter Jansson, Regine Hock, and Thomas Schneider, "The Concept of Glacier Storage: A Review," *Journal of Hydrology*, vol. 282, no. 1-4, pp. 116-129, 2003. [CrossRef] [Google Scholar] [Publisher Link]

[4] W. Nigel Arnell et al., *Hydrology and Water Resources*, Cambridge University Press, pp. 1-1032, 2001. [Google Scholar] [Publisher Link]

[5] J.T. Houghton et al., *Climate Change 2001: The Scientific Basis, Contribution of Working Group I to the Third Assessment Report of the Intergovernmental Panel on Climate Change*," IPCC, pp. 1-893, 2001. [Google Scholar] [Publisher Link]

[6] Martin Parry et al., "*Climate Change 2007: Impacts, Adaptation and Vulnerability: Contribution of Working Group II to the Fourth Assessment Report of the Intergovernmental Panel on Climate Change*," IPCC, pp. 1-987, 2007. [Google Scholar] [Publisher Link]

[7] Daniel Viviroli et al., "Mountains of the World, Water Towers for Humanity: Typology, Mapping, and Global Significance," *Water Resources Research*, vol. 43, no. 7, pp. 1-13, 2007. [CrossRef] [Google Scholar] [Publisher Link]

[8] W.W. Immerzeel, F. Pellicciotti, and M.F.P. Bierkens, "Rising River Flows throughout the Twenty-First Century in Two Himalayan Glacierized Watersheds," *Nature Geoscience*, vol. 6, pp. 742-745, 2013. [CrossRef] [Google Scholar] [Publisher Link]

[9] Silvan Ragettli, Walter W. Immerzeel, and Francesca Pellicciotti, "Contrasting Climate Change Impact on River Flows from High-Altitude Catchments in the Himalayan and Andes Mountains," *Proceedings of the National Academy of Sciences*, vol. 113, no. 33, pp. 9222-9227, 2016. [CrossRef] [Google Scholar] [Publisher Link]

[10] Matthias Huss, and Regine Hock, "Global-Scale Hydrological Response to Future Glacier Mass Loss," *Nature Climate Change*, vol. 8, pp. 135-140, 2018. [CrossRef] [Google Scholar] [Publisher Link]

[11] Hamish D. Pritchard, "Asia's Glaciers are a Regionally Important Buffer against Drought," *Nature*, vol. 545, pp. 169-174, 2017. [CrossRef] [Google Scholar] [Publisher Link]

[12] Lorenzo Alfieri et al., "High-Resolution Satellite Products Improve Hydrological Modeling in Northern Italy," *Hydrology and Earth System Sciences Discussions*, vol. 26, no. 14, pp. 3921-3939, 2021. [CrossRef] [Google Scholar] [Publisher Link]

[13] Xiaofeng Wang et al., "Evaluation and Comparison of Reanalysis Data for Runoff Simulation in the Data-Scarce Watersheds of Alpine Regions," *Remote Sensing*, vol. 16, no. 5, pp. 1-21, 2024. [CrossRef] [Google Scholar] [Publisher Link]

[14] J. Martinec, "Snowmelt - Runoff Model for Stream Flow Forecasts," *Hydrology Research*, vol. 6, no. 3, pp. 145-154, 1975. [CrossRef] [Google Scholar] [Publisher Link]

[15] Sarita Tiwari, Sarat C. Kar, and R. Bhatla, "Snowfall and Snowmelt Variability over Himalayan Region in Inter-Annual Timescale," *Aquatic Procedia*, vol. 4, pp. 942-949, 2015. [CrossRef] [Google Scholar] [Publisher Link]

[16] Sonia Grover et al., "Modeling Hydrological Processes in Ungauged Snow-Fed Catchment of Western Himalaya," *Water Resources*, vol. 47, pp. 987-995, 2020. [CrossRef] [Google Scholar] [Publisher Link]

[17] Kuldeep Singh Rautela et al., "Long-Term Hydrological Simulation for the Estimation of Snowmelt Contribution of Alaknanda River Basin, Uttarakhand Using SWAT," *AQUA-Water Infrastructure, Ecosystems and Society*, vol. 72, no. 2, pp. 139-159, 2023. [CrossRef] [Google Scholar] [Publisher Link]

[18] Aditya Mishra et al., "Glacier Inventory and Glacier Changes (1994-2020) in the Upper Alaknanda Basin, Central Himalaya," *Journal of Glaciology*, vol. 69, no. 275, pp. 591-606, 2023. [CrossRef] [Google Scholar] [Publisher Link]

[19] Maheswor Shrestha et al., "Integrated Simulation of Snow and Glacier Melt in Water and Energy Balance-Based, Distributed Hydrological Modeling Framework at Hunza River Basin of Pakistan Karakoram Region," *Journal of Geophysical Research: Atmospheres*, vol. 120, no. 10, pp. 4889-4919, 2015. [CrossRef] [Google Scholar] [Publisher Link]

[20] Rosanna A. Lane et al., "Benchmarking the Predictive Capability of Hydrological Models for River Flow and Flood Peak Predictions Across over 1000 Catchments in Great Britain," *Hydrology and Earth System Sciences*, vol. 23, no. 10, pp. 4011-4032, 2019. [CrossRef] [Google Scholar] [Publisher Link]

[21] Shuai Zhou et al., "Quantifying the Uncertainty Interaction between the Model Input and Structure on Hydrological Processes," *Water Resources Management*, vol. 35, pp. 3915-3935, 2021. [CrossRef] [Google Scholar] [Publisher Link]

[22] Jeff Dozier et al., "Time-Space Continuity of Daily Maps of Fractional Snow Cover and Albedo from MODIS," *Advances in Water Resources*, vol. 31, no. 11, pp. 1515-1526, 2008. [CrossRef] [Google Scholar] [Publisher Link]

[23] Mark G. Flanner et al., "Present-Day Climate Forcing and Response from Black Carbon in Snow," *Journal of Geophysical Research: Atmospheres*, vol. 112, no. D11, pp. 1-17, 2007. [CrossRef] [Google Scholar] [Publisher Link]

[24] Jing Ming et al., "An Overview of Black Carbon Deposition in High Asia Glaciers and its Impacts on Radiation Balance," *Advances in Water Resources*, vol. 55, pp. 80-87, 2013. [CrossRef] [Google Scholar] [Publisher Link]

[25] Chaman Gul et al., "Concentrations and Source Regions of Light-Absorbing Particles in Snow/Ice in Northern Pakistan and their Impact on Snow Albedo," *Atmospheric Chemistry and Physics*, vol. 18, no. 7, pp. 4981-5000, 2018. [CrossRef] [Google Scholar] [Publisher Link]

[26] Hans Hersbach et al., "The ERA5 Global Reanalysis," *Quarterly Journal of the Royal Meteorological Society*, vol. 146, no. 730, pp. 1999-2049, 2020. [CrossRef] [Google Scholar] [Publisher Link]

[27] Raul R. Wood et al., "Comparison of High-Resolution Climate Reanalysis Datasets for Hydro-Climatic Impact Studies," *EGUsphere*, pp. 1-41, 2024. [CrossRef] [Google Scholar] [Publisher Link]

[28] J.I. López-Moreno et al., "Different Sensitivities of Snowpacks to Warming in Mediterranean Climate Mountain Areas," *Environmental Research Letters*, vol. 12, no. 7, pp. 1-10, 2017. [CrossRef] [Google Scholar] [Publisher Link]

[29] Kuldeep Singh Rautela et al., "Estimation of Stream Hydraulic Parameters and Suspended Sediment Load of River Neola in the Foothills of the Panchachuli Glacier during the Ablation Period," *Journal of Himalayan Ecology and Sustainable Development*, vol. 15, pp. 114-125, 2020. [Google Scholar] [Publisher Link]

[30] Kuldeep Singh Rautela et al., "Assessment of Daily Streamflow, Sediment Fluxes, and Erosion Rate of a Pro-Glacial Stream Basin, Central Himalaya, Uttarakhand," *Water, Air, and Soil Pollution*, vol. 233, 2022. [CrossRef] [Google Scholar] [Publisher Link]

[31] T. Bolch et al., "The State and Fate of Himalayan Glaciers," *Science*, vol. 336, no. 6079, pp. 310-314, 2012. [CrossRef] [Google Scholar] [Publisher Link]

[32] Bodo Bookhagen, and Douglas W. Burbank, "Toward a Complete Himalayan Hydrological Budget: Spatiotemporal Distribution of Snowmelt and Rainfall and their Impact on River Discharge," *Journal of Geophysical Research: Earth Surface*, vol. 115, no. F3, pp. 1-25, 2010. [CrossRef] [Google Scholar] [Publisher Link]

[33] Abhilash Gogineni, Madhusudana Rao Chintalacheruvu, and Ravindra Vitthal Kale, "Modelling of Snow and Glacier Melt Dynamics in a Mountainous River Basin Using Integrated SWAT and Machine Learning Approaches," *Earth Science Informatics*, vol. 17, pp. 4315-4337, 2024. [CrossRef] [Google Scholar] [Publisher Link]

[34] A.F. Lutz et al., "Consistent Increase in High Asia's Runoff due to Increasing Glacier Melt and Precipitation," *Nature Climate Change*, vol. 4, pp. 587-592, 2014. [CrossRef] [Google Scholar] [Publisher Link]

[35] Meng Zhang et al., "Automated Glacier Extraction Index by Optimization of Red/SWIR and NIR /SWIR Ratio Index for Glacier Mapping Using Landsat Imagery," *Water*, vol. 11, no. 6, pp. 1-24, 2019. [CrossRef] [Google Scholar] [Publisher Link]

[36] Regine Hock et al., "Glacier Melt: A Review of Processes and their Modelling," *Progress in Physical Geography: Earth and Environment*, vol. 29, no. 3, pp. 362-391, 2005. [CrossRef] [Google Scholar] [Publisher Link]

[37] K. Amrutha et al., *Climate Change Impact on Major River Basins in the Indian Himalayan Region: Risk Assessment and Sustainable Management*, Climate Change Adaptation, Risk Management and Sustainable Practices in the Himalaya, Springer, Cham, pp. 45-63, 2023. [CrossRef] [Google Scholar] [Publisher Link]

[38] "*Climate Change 2021-The Physical Science Basis, Working Group I Contribution to the Sixth Assessment Report of the Intergovernmental Panel on Climate Change*," Intergovernmental Panel on Climate Change (IPCC), Cambridge University Press, 2023. [CrossRef] [Publisher Link]

[39] Poonam Vishwas, K.C. Tiwari, and Gopinadh Rongali, "Mapping Glacial Lakes and Glacial Lake Outburst Floods in the Alaknanda River Basin, Uttarakhand: A Remote Sensing and GIS-Based Approach," *Indian Journals*, vol. 10, no. 1, pp. 1-17, 2023. [CrossRef] [Google Scholar] [Publisher Link]

[40] Luca Cossa et al., "The Role of Snowpack Dynamics in Seasonal Water Supply Variability," *Hydrology: Current Research*, vol. 15, no. 3, pp. 1-2, 2024. [Publisher Link]